A Conceptual Design Study of a Compact Photon Source (CPS) for Jefferson Lab

E. Chudakov,[1] D. Day,[2] P. Degtiarenko,[1] R. Ent,[1] D.J. Hamilton,[3] T. Horn,[4,1,*] D. Keller,[2] C. Keppel,[1] G. Niculescu,[5] P. Reid,[6] I. Strakovsky,[7] B. Wojtsekhowski,[1] and J. Zhang[2]

[1] *Jefferson Lab*
[2] *University of Virginia*
[3] *University of Glasgow*
[4] *Catholic University of America*
[5] *James Madison University*
[6] *Saint Mary's University*
[7] *George Washington University*

(Dated: July 1, 2019)

This document describes the technical design concept of a compact, high intensity photon source (CPS) to be used with dynamically nuclear polarized targets. The novel CPS technique unlocks access to physics processes with very small scattering probabilities that is not possible with currently existing facilities. Capable of producing 10^{12} equivalent photons per second, the deployment of the CPS will result in a large gain in polarized experiment figure-of-merit (by a factor of $\sim$30). Compared to a traditional bremsstrahlung photon source the proposed solution will present several advantages, including much lower radiation levels, both prompt and post-operational due to the beam line elements radio-activation. For use with polarized targets, the heat load and radiation damage effects are well within the acceptable range.

Keywords: photon source

I Introduction

Traditionally, knowledge has been gathered on the structure of protons and neutrons from studies of their static properties (mass and spin, polarizabilities, form factors) and the one-dimensional quark and gluon momentum distributions underlying them. Yet despite decades of research, our knowledge of the microcosm of proton structure has remained elusive.

Just as the earth orbits around the Sun while simultaneously spinning about its own axis, the quarks and gluons in a proton could have linear motion, orbital motion, and spin, the latter two responsible for the overall proton spin that is exploited daily in thousands of MRI images worldwide. But, well beyond this classical analogy in the proton's quantum mechanical microcosm quark and gluon constituents are dynamic, they can appear and disappear (that is, beyond a very few ever-prevalent "valence" quarks that define the proton's identity), and all strongly interact. In fact, unlike with the more familiar atomic and molecular matter, interactions and structures in nuclear matter are inextricably mixed up, and the observed properties of nucleons and nuclei, such as mass and spin, emerge out of this complex system.

Realization has grown that the true study of the proton dynamical structure has to come from more exclusive reactions, processes in which the deep inside of the proton is studied with a highly-energetic photon or electron probe by a completely-measured set of only a few particles. Even though the scattering probability of such reactions is minuscule[1] realization has dawned that such more exclusive "designer" reactions have a much closer connection to imaging and understanding the elusive 3D proton substructure. Indeed, there have been increasingly sophisticated theoretical efforts to exploit the richness of exclusive reactions at moderate resolution scales (or momentum transfer). This mimics progress in other fields of science, where imaging the physical systems under study has been key to gaining new understanding, with as prominent examples the progress in understanding since advent of X-ray diffraction in the 1920's or the advent of large-scale cosmological surveys in the 2000's.

High-energy photon beam experiments leading to a final state of a completely-measured set of only a few particles allow, in complementary fashion to high-energy electron beam experiments, to image the deep inside structure of the proton. This is the topic of a new science direction termed "nuclear femtography". Unlike electron scattering experiments, where the "camera" resolution scale is set by the four-momentum transfer squared, Q^2, and its shutter speed by the energy transferred, for photon beam experiments the four-momentum transferred to the proton target, $-t$, and the total energy, s, set the resolution scale and shutter

*Contact email:hornt@cua.edu

[1] It is much easier for the highly energetic electron probe to use its energy to break the proton apart

speed of the proton images. This allows, in principle, under the right resolution and shutter speed conditions, to disentangle four functions representing the vector, axial, tensor, and pseudo-scalar response of the nuclear system, the proton H, $\tilde{H}$, E and $\tilde{E}$. These functions need to be modeled and constrained with parameters extracted from experimental data. This all can be easiest achieved by also including polarization degrees of freedom, most readily by polarizing the nuclear system under study.

Much progress to image proton structure can be made with electron-scattering reactions. Yet, experiments utilizing high-energy photons will play a unique complementary science role. But, to measure the small scattering probabilities related to exclusive reactions demands high-intensity photon beams. Further, our basic understanding will be much strengthened by imaging longitudinally-polarized (along the photon beam direction) and transversely-polarized (transverse to this) protons. It is for this combination that our new comcept is so unique: with a new-developed Compact Photon Source and a dynamically-nuclear polarized target system, we gain a factor of 30 in the Figure-Of-Merit (as defined by the photon intensity and the average target polarization over the experiment). This gain could be further doubles by use of a novel magnet system to polarize targets with much larger particle detection acceptance than previously possible. The net gain opens the window on the minuscule scattering probabilities associated with a new suite of high-energy photon scattering experiments to image and understand the dynamical proton structure. The basic technique to establish the Compact Photon Source (CPS) also enables other science, e.g. by using the source to create a beam of neutral kaons.

This document is organized as follows. In section II, we give a short overview of the possible science gain enabled by the CPS, using two examples. In section III, we outline the generic idea behind the novel CPS design as compared to the more traditional photon beam methods. In section IV, the conceptual design and component details of the CPS are presented. Section V lists the requirements a CPS has to meet to fulfill operational dose rates at Jefferson Lab. In section VI, we discuss the results of our shielding design and optimization studies and compare them with the requirements in section V. Finally, section VII deals with engineering and safety aspects including material considerations, and secrtion 'refsec:summary summarizes the Compact Photon Source design features and performance.

II Science Gain with CPS

Investigating the three-dimensional structure of the nucleon has been an active and productive field of research especially during the last two decades since the invention of the so-called Generalized Parton Distributions (GPD) formalism. Studies towards this three-dimensional structure, or nuclear femtography, continue to be central to the hadron physics program at JLab. The GPD formalism provides a unified description of several important reactions such as elastic electron scattering, Deep-Inelastic Scattering (DIS), Deeply-Virtual and Timelike Compton Scattering (DVCS and TCS), Deeply-Virtual Meson Production (DVMP), and Wide-Angle Real Compton Scattering (RCS) and meson production, which can all be described by a single set of four functions H, $\tilde{H}$, E and $\tilde{E}$. These functions need to be modeled and constrained with parameters extracted from experimental data.

The CPS and the physics it enables would provide a complementary tool, using photon beams next to electron beams, to address this priority-goal in the hadronic physics community. The Jefferson Lab Program Advisory Committee has endorsed this view, and fully approved one and conditionally approved another experiment that require the CPS. Below, we shortly describe these two experiments.

E12-17-008 [6]: Polarization Observables in Real Compton Scattering (A-rated, 45 PAC days, spokespersons: D. Hamilton, D. Day, D. Keller, G. Niculescu, B. Wojtsekhowski, J. Zhang) When a photon probe is used to study the proton, with in the final state one energetic photon and the proton remaining, the process is called Real Compton Scattering (RCS). This is a fundamental and basic process, yet its mechanism in the center-of-mass energy regime of $\sqrt{s}$ = 5-10 GeV remains poorly understood. Measurements show that these data cannot be described by perturbative calculations involving the scattering of three valence quarks, but that the dominant mechanism could be the so-called "handbag model" where the photon scatters of a single quark, and convoluted with a coupling of this struck quark to the spectator system is described by so-called Generalized Parton Distributions (GPDs). It is this latter conceptual mechanism that lies at the root of the worldwide efforts of 3D (spatial) imaging of the proton's quark-gluon substructure, as the GPDs contain information about the transverse spatial distribution of quarks and their longitudinal momenta inside the proton.

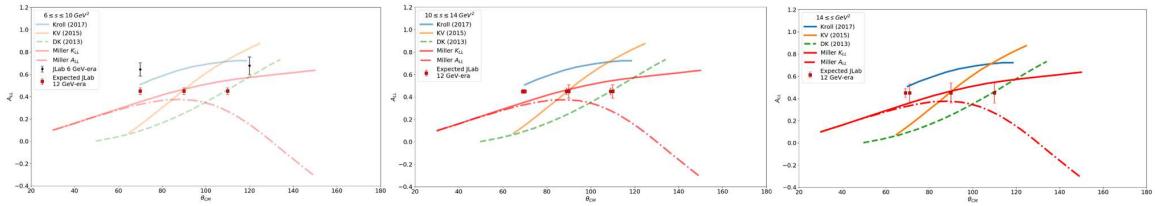

Figure 1: *Existing Real Compton Scattering (RCS) models show a large variation in the expected initial-state Asymmetry, A_{LL}. The only two existing JLab 6 GeV-era measurements [10] (black symbols) lie in a region where the models are not yet applicable. This is indicated by the lighter color of the lines in the left panel. Also shown are the anticipated data points to be measured at JLab using the CPS (middle and right panel). These points will provide essential experimental confirmation and constraints on GPD models.*

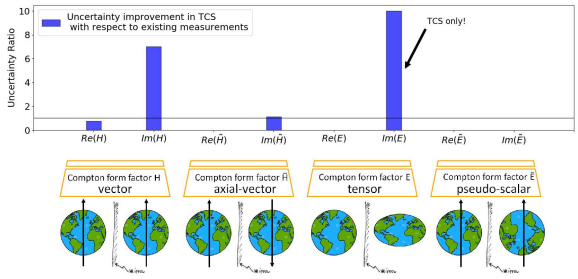

Figure 2: *The expected improvement in the uncertainties in extracting the Compton Form Factors pertaining to various GPDs using Timelike Compton Scattering (TCS) compared to the uncertainties stemming from DVCS-based extraction alone. The various cartoons and their mirror symmetries illustrate various aspects that can be derived on the 3D (spatial) images of subatomic matter. Note that while providing an independent check of universality and improvement on the DVCS data, TCS offers unique new access to the elusive "E" GPD.*

The RCS experimental observables provide several constraints for GPDs which are complementary to other exclusive reactions due to an e_a^2 factor and an additional $1/x$ weighting in the GPD integrals for RCS. For example, the elastic form factor $F_1(t) = \sum_a e_a \int dx H^a(x,0,t)$ is related to the RCS vector form factor $R_V(t) = \sum_a e_a^2 \int \frac{dx}{x} H^a(x,0,t)$, both of which are based on the same underlying GPD $H(x,0,t)$. Similarly, polarized observables in RCS uniquely provide high $-t$ constraints on $\tilde{H}(x,\xi,t)$ via extraction of the RCS axial form factor $R_A(t)$ in a kinematic regime where precise data on the nucleon axial form factor is not available.

A measurement of the spin asymmetry in RCS with the proton target longitudinally polarized can further disentangle the existing handbag mechanisms. If consistent with the measurement of the spin transfer from the photon to the scattered proton, the asymmetry can indeed be surprisingly large and stable with respect to the photon center-of-mass scattering angle. Such investigations into the mechanisms behind RCS will provide crucial insight into the nature of exclusive reactions and proton structure and are ideally suited for the facilities provided by the Jefferson Lab 12-GeV upgrade.

C12-18-005 [7] (conditionally approved, 46 PAC days, spokespeople: M. Boer, D. Keller, V. Tadevosyan) When a real photon is scattered off a quark of the proton and a high-mass (virtual) photon is emitted, then decays into a lepton pair, the process is called Timelike Compton Scattering (TCS). Using a transversely polarized proton target and a real circularly polarized photon beam, we can access several independent observables directly sensitive to the GPDs, and in particular the GPD E which is poorly constrained and of great interest due to its relation with the orbital momentum of the quarks. We plan to measure the unpolarized scattering probabilities or cross section, the cross section using circularly polarized photon beam, and the cross sections using transversely-polarized protons. This together also provides a first fundamental test of the universality of the GPDs, as the GPDs extracted from TCS should be comparable with those that will be extracted from the analogous spacelike (electron) scattering process - Deeply Virtual Compton Scattering, a flagship program of the 12-GeV Jefferson Lab Upgrade.

III Science Method

CEBAF is the world's most advanced electron accelerator for investigating the nucleus of the atom, the protons and neutrons making up the nucleus, and the 3D structure of quarks and gluons inside them. It has been realized that exclusive reactions, leading to a final state of a

completely-measured set of only a few particles, have a much closer connection to this 3D structure. High-energy photoproduction provides unique and complementary access to electron scattering to image this elusive 3D structure deep inside the proton. Fig. 3c shows the novel CPS solution that provides the high-intensity photons, with a unique factor 30 gain in Figure-Of-Merit (see Fig. 4), to unlock access to these reactions with very small scattering probabilities, not possible with currently existing facilities.

A traditional source of high-energy photons comes from an electron beam hitting a radiator, most common Cu, producing a cone of bremsstrahlung photons accompanying the electron beam (see Fig. 3a). The photon and ongoing electron beam spread is dominated by electron multiple scattering, and for electron beam energies of a few GeV is typically less than 1 mrad. Accompanying this mixed photon and electron beam is a much larger angular distribution of secondary particles produced in the electron-nuclei shower. For example, the cone of secondary particles that survive filtering through a heavy absorber material of one nuclear interaction length (≈140-190 g/cm^2 or ≈15 cm) has an angular spread of 100-1000 mrad. Even if this method can produce the largest flux of photons, drawbacks are that the beam is a mix of photons and electrons, that the photon beam energy is not a priori known, and that the method is accompanied with large radiation background doses due to the large spread of secondary particles produced.

An alternate method to produce a (pure) photon beam includes a radiator, a deflection magnet and a beam dump for the undeflected electrons, augmented for energy-tagged photon beams with a set of focal plane detectors covering a modest to large momentum acceptance (see Fig. 3b). Such a configuration requires significant space along the beam direction and heavy shielding around the magnet and the beam dump, which have large openings due to the large angular and energy spread of the electrons after interaction with the radiator. In addition, without tight collimation the traditional scheme leads to a large size of the photon beam at the target due to divergence of the photon beam and the long path from the radiator to the target. This can be an issue as the beam spot size contributes to the angular and momentum reconstruction resolution of the resultant reaction products due to uncertainty in the transverse vertex position. As an example, to obtain the needed reconstruction resolution of the scattered photon in RCS the photon spot size at the target must be equal or less than 2 mm. This would require the target to be at a distance of 2 meters from the radiator, which is often practically impossible. The advantage of this method is that one has a pure photon beam, and if augmented with a set of focal-plane tagging detectors the exact photon energies can be determined. Drawback is that to accomplish this the flux of incident electrons, and thus the photon flux, has to be drastically reduced, especially when the tagging method is used. Similarly, this scheme also comes with appreciable radiation doses, especially with increased photon fluxes, as particles are allowed to propagate over short distances before mitigation of radiation by containment starts to be effective.

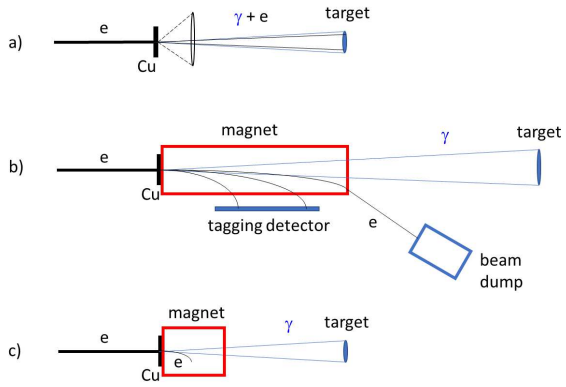

Figure 3: *Different schemes to produce high-energy photon beams. Scheme a) is the traditional bremsstrahlung technique where a Cu radiator is placed in an electron beam to render a mixed photon and electron beam. In scheme b) a deflection magnet and beam dump are used to peel off the electrons and produce a photon-only beam. Scheme c) is the new Compact Photon Source technique, with a compact combined magnet-electron dump and a narrow photon-only beam.*

The CPS (see Fig. 3c) addresses the shortcomings of these two traditional techniques. The concept of the CPS takes advantage of the narrowness of the photon beam relative to the angular distribution of the secondary particles produced in the electron-nuclei shower. The CPS combines in a single shielded assembly all elements necessary for the production of the intense photon beam and ensures that the operational radiation dose rates around it are acceptable (see Ref. [11]). Much of this is achieved by keeping the overall dimensions of the setup limited, and by careful choice and ordering of materials. The CPS design features a magnet, a central copper absorber to handle the power deposition, and tungsten powder and borated plastic to hermetically shield the induced radiation doses as close to the source as possible.

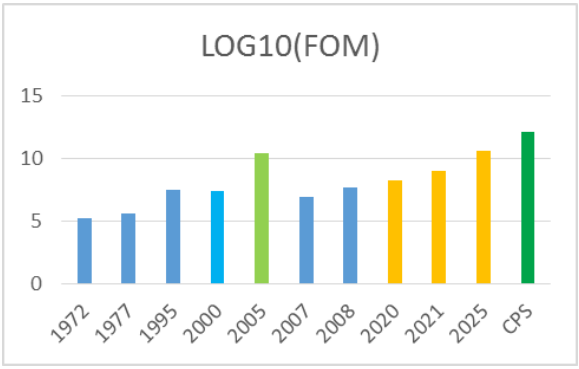

Figure 4: *The Figure-Of-Merit (FOM) of photon beam experiments with Dynamically Nuclear Polarized targets, defined as the logarithm of the effective photon beam intensity times the averaged target polarization squared, as a function of time. Note the large gain, over a factor of 30 as compared to any setup, enabled by the CPS. The vertical axis is log scale. The indicated FOM in 1972, 1977, 1995, 2007 and 2008 are based on actual experiments at Daresbury, Bonn, Jefferson Lab and Mainz [14–16]. The FOM noted in 2000 and 2005 are based upon proposed setups at SLAC and Jefferson Lab, with the latter closest in concept to the CPS. We also add the projected FOM of approved future experiments at HiGS/Duke and Jefferson Lab.*

The magnet acts as dump for the electrons with a cone of photons escaping through a small collimator without loss of intensity. The size of the collimator can be as narrow as the photon beam size with natural divergence plus the size of the beam raster. The combined magnet-dump thus allows for dramatically reducing the magnet aperture and length, as well as the weight of the radiation shield, due to the compactness of the source and minimization of openings, thus reducing radiation leakage. This opens a practical way forward with management of both the radiation environment in the magnet and the power deposition density in the copper absorber.

Compared to the more traditional bremsstrahlung photon sources (Figs. 3a and 3b and *e.g.* Refs. [12, 13]), the proposed solution offers several advantages, including an intense and narrow photon-only beam and much lower radiation levels, both prompt and post-operational due to the beam line elements radio-activation. The drawbacks are a somewhat reduced photon flux as compared to the scheme of Fig. 3a, and not having with a focal plane detection option the ability to directly measure the photon energy as in the scheme of Fig. 3b.

The primary gain of the CPS is for experiments using Dynamically Nuclear Polarized (DNP) Targets, with an estimated gain in Figure-Of-Merit of a factor of 30. Dynamic Nuclear Polarization is a technique to provide an effective way to produce polarized protons. Here, a material containing a large fraction of protons is cooled to low temperatures, <1K, and placed in a strong magnetic field, typically about 5 Tesla. These conditions cause the electrons to self-polarize, and their polarization is then transferred to the proton using microwave techniques. These conditions however at the same time impose a serious limitation. Beams traversing the polarized target material will produce ionization energy losses warming and depolarizing the target. It also produces harmful free radicals which allow pathways for the proton polarized to decay. This limits the (local) beam intensities the polarized target material can handle.

Conventional target cells have diameters much larger than the desirable beam spot size, and one is forced to minimize rapid degradation of the target polarization by the beam, induced by either heat deposition or ionizing radiation, at one location at the target. The traditional solution of minimizing such localized polarization degradation is fast movement of the beam spot, which allows avoiding overheating of the material and equalizing of the degradation over the target volume. A beam raster magnet, which moves the beam with a frequency of several Hz, was used in past experiments at Hall C. However, this does not work for very small apertures, e.g. a few mm by a few mm collimation cone, limiting possible beam motion. The CPS solution for the beam-target raster thus includes a combination of the target rotation around the horizontal axis and ± 10 mm vertical motion of the target ladder. Such a raster method effectively moves the motion complexity out of the high radiation area of the absorber. The same effect can be achieved by vertical displacement of the beam spot, i.e. by a small variation of the vertical incident angle of the electron beam at the radiator. With a ± 5 mrad vertical angle variation and 200 cm distance between the radiator and the target, the displacement of the beam spot is equal to ± 1 cm, about the size of the conventional target cells. Traditionally, such photon beam experiments have been performed using the scheme indicated in Fig. 3a. This limits the electron beam current to less than 100 nA to prevent rapid target polarization damage. With the CPS scheme, we anticipate use of an electron beam current of up to 2.7 μA to provide the photon flux for an equivalent heat load in the DNP target. Hence, we gain a factor of about 30. The history of the Figure-Of-Merit of bremsstrahlung photon beam experiments with DNP targets is further illustrated in Fig. 4.

IV The Compact Photon Source - Description of Instrumentation

The physics program described requires a high-intensity and narrow photon beam and a polarized target to access the exclusive photoproduction reactions to extract the polarized target observables. The CPS provides a compact solution with a photon flux of 1.5×10^{12} equivalent photons/s, with a factor of 1000 reduction in prompt radiation dose compared to a 2.7 μA (30 kW) electron beam current striking a 10% Cu radiator. The CPS meets the acceptable radiation level requirements for a typical run time of 1000 hours at Jefferson Lab with the photon source located at 2-3m from the target. The polarized target requirements are fulfilled with a novel rotating polarized target cell combined with a dynamic nuclear polarization (DNP) system.

A Conceptual Design

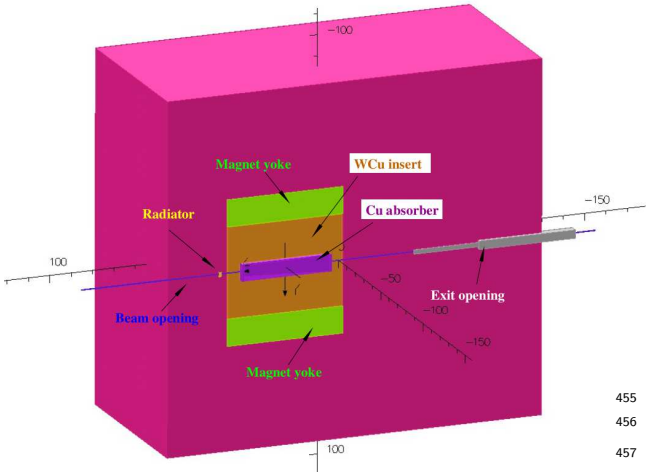

Figure 5: The CPS cut-off view. Most of the deflected electrons strike a copper absorber, surrounded by a W-Cu insert inside the magnet yoke. The outer rectangular region in this view is the tungsten-powder shield.

The main elements of the CPS are shown in Figure 5. Without loss of photon intensity, a channel (a collimator for the secondary radiation but not for the photon beam) around the photon beam could be as narrow as the photon beam size with natural divergence plus the size of the beam raster. After passing through the radiator, the electron beam should be removed from the photon line by means of a magnet. The length, aperture and field of the magnet are very different in the proposed source from the traditional one. In the traditional source the magnet is needed to direct the electrons to the dump. Because of the large momentum spread of electrons which have interacted in the radiator, the magnet aperture needs to be big and the dump entrance should be even bigger: 13% of the beam power would be lost before the beam dump, even with a 10% momentum acceptance of the beam line. In contrast, in the proposed source the magnet acts as dump for the electrons with a cone of photons escaping through a small collimator.

The electron energy dumping starts on the side of the photon beam channel, so a shift of the electron trajectory by just 1-3 mm is already sufficient for the start of the shower. At the same time, such a deflection needs to be accomplished at a relatively short distance (much shorter than the size of the radiation shielding) after the beam passes through the radiator to keep the source compact. Indeed, with a deflection radius, R, a vertical size of the channel, $2a$, and a vertical raster size, $2b$, the trajectory enters the channel side after traveling in the magnetic field a distance, p, which varies from $p = \sqrt{2\,R\,(a-b)}$ to $p = \sqrt{2\,R\,(a+b)}$ (see the scheme in Figure 6). In the currently proposed

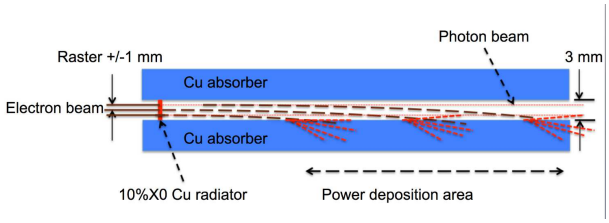

Figure 6: The scheme of beam deflection to the absorber/dump.

CPS magnet the trajectory radius R is about 10 m for 11 GeV electrons, the channel size is 0.3 cm, and the raster size is 0.2 cm, so the distance p has an average value of 17 cm with a spread of 12 cm. A total field integral of 1000 kG-cm is adequate for our case, which requires a 50 cm long iron dominated magnet.

The above concept of the combined magnet-dump allows us to reduce dramatically the magnet aperture and length, as well as the weight of the radiation shield, due to the compactness of the source and minimization of openings, thus significantly reducing the radiation leakage. Such a conceptual design opens a practical way forward for a CPS, providing one can manage both the radiation en-

vironment in the magnet and the power deposition density in the copper absorber.

B Magnet

Normal conducting magnets for operation in high levels of radiation have been constructed at several hadron facilities, including the neutron spallation source at ORNL and the proton complex JPARC. We designed the magnet with permendur poles tapered in two dimensions, which allows us to reach a strong magnetic field at the upstream end of the magnet (3.2 Tesla), with the coils located 20 cm from the source of radiation. The resulting radiation level at the coil location is calculated to be low enough, below 1 Mrem/hr, to allow the use of a modest-cost kapton tape based insulation of the coils. The length of the magnet was selected to be 50 cm and the field integral 1000 kG-cm. Figure 7 shows the longitudinal profile of the magnetic field obtained from OPERA calculations.

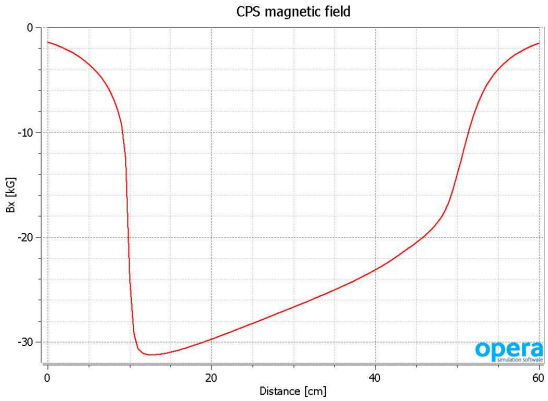

Figure 7: Magnetic field (B_x) profile along the beam direction, as a distance from the radiator position.

C Central Absorber

The beam power is deposited in an absorber made of copper, whose high heat conductivity helps to manage the power density. An absorber made of aluminum would help to reduce power density by a factor of 2-3 compared with copper due to its smaller radiation length, but it would also increase the length of the CPS by about 50 cm so is not preferred. The heat removal from the copper absorber is arranged first via heat conductivity to the wider area where water cooling tubes are located. Figure 8 shows the longitudinal profile of the power density according to the MC simulation.

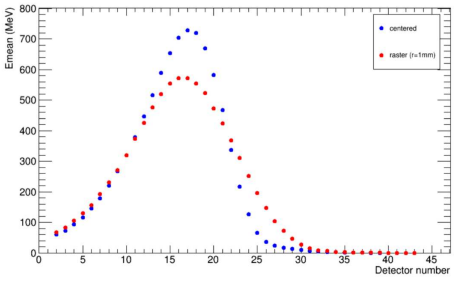

Figure 8: Longitudinal profile of the energy distribution (integrated for one cm copper slab) for a single 11 GeV incident electron. The maximum power density is occurs at a distance of 18 cm from the radiator. The blue dots show the energy deposition for the electron beam centered in a 3 mm by 3 mm channel. The red dots show the same for the beam rastered with a radius of one mm.

The transverse distribution of power is also very important to take into account because, for a high energy incident beam, it has a narrow peak. A detailed MC simulation of the deposited power density and the 2-dimensional heat flow analysis were performed to evaluate the maximum temperature in the copper absorber. Figure 9 (left panel) shows the layout of materials in the model used for the temperature analysis. The calculation was performed for the case of a 11 GeV 30 kW beam and a 10% X0 radiator, and the temperature was found to be below 400°C, which is well in the acceptable range for copper. Figure 9 (right panel) shows the temperature profile in the transverse plane at the longitudinal location of maximum power deposition. Cooling of the core will require about four gallons of water per minute at 110 psi pressure (at 30°C temperature rise), which is easy to provide.

D Tungsten-powder Shield

The amount of material needed for radiation shielding is primarily defined by the neutron attenuation length, which is 30 g/cm^2 for neutrons with energy below 20 MeV and 125 g/cm^2 for high energy neutrons. The neutron production rate by an electron beam in copper is 1×10^{12} per kW of beam power according to a SLAC report (W.P. Swanson, SLAC-PUB 2042, 1977, see Figure 10). At a distance of 16 meters from the unshielded source for a 30 kW beam, the neutron flux would be 1×10^7 n/cm^2/s, which would produce a radiation level of 110 rem/hr, or 850 times higher than during the RCS experiment at JLab (E99-114) (at

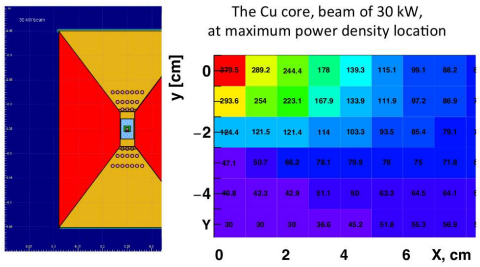

Figure 9: Left panel: the cross section of the absorber (shown in blue (copper) in the center and yellow (W-Cu(20%)) surrounding) with the water cooling channels. Right panel: the temperature map for 1 cm by 1 cm elements at the longitudinal coordinate of the power deposition maximum.

a 16-meter distance from the pivot in the upstream direction). The current conceptual design with a total shield mass of 850 g/cm^2 will result in reduction in these radiation levels by a factor of 1000.

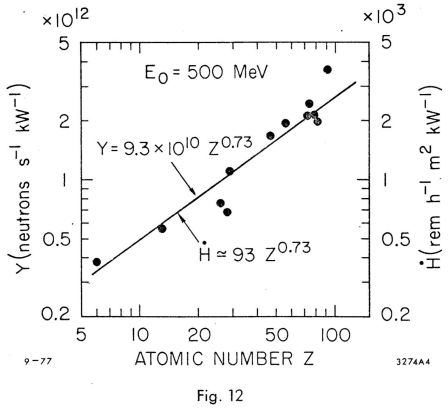

Fig. 12

Figure 10: The neutron yield according to SLAC-PUB 2042.

The space inside the magnet between the poles and coils is filled by an inner copper absorber and an outer W-Cu(20%) insert, which provides a good balance between effective beam power absorption and radiation shielding. For the shield outside the magnet, the current design uses tungsten powder, whose high density (16.3 g/cm^3) helps to reduce the total weight of the device. A thickness of 50 cm was used as a first iteration for the thickness of the outer shield of the CPS, but we have investigated the impact of varying this amount of outer shielding (as discussed later in the document).

E Impact on Polarized Target

The most significant gain associated with deployment of the CPS is for experiments using dynamically polarized targets. However, such polarized targets operate with strong 2.5-5 Tesla polarizing fields themselves. In addition, dynamically polarized target operation imposes strict requirements on the field quality at the target location, where fields and gradients need to be compensated at the 10^{-4} level. This necessitates studies of the mutual forces associated with the 2-3 Tesla CPS dipole magnet and the 5 Tesla polarized target solenoid, in terms of both the design of the support structures and the operation of the polarized target.

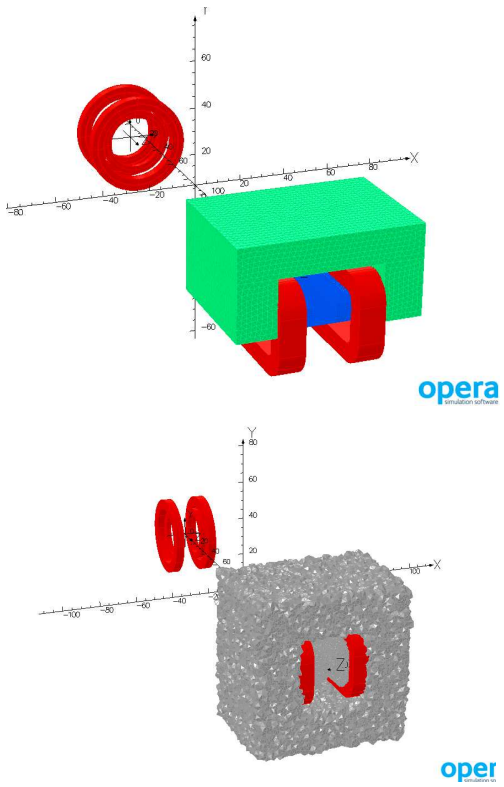

Figure 11: The TOSCA model used in the field and force calculations, for longitudinal orientattion of the coils/target polarization (left) and transverse orientation (right).

The fields associated with the combination of these two magnetic systems were calculated using the model shown in Figure 11 (left panel, for the polarized target configured for longitudinal polarization), with the following results obtained:

- When the CPS is ON but the polarized target magnet is OFF, the (total) field at

the target location amounts to only about 0.1 Gauss.

- When the polarized target magnet is on and the CPS is OFF or removed, the field at the CPS location is about 130 Gauss.

- When both the CPS is ON and the polarized target magnet is ON, the field gradient at the polarized target center is about 2 Gauss/cm (Figure 12).

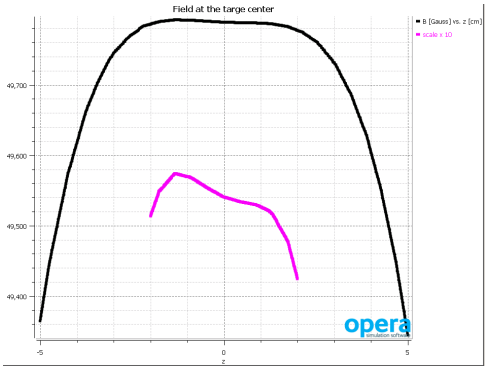

Figure 12: The field at the target center. Insert shows a field zoomed by a factor of 10. Values of the field (B) in Gauss and the coordinate (z) in cm.

These results show that, for the CPS the induced field is mainly due to the CPS magnet yoke becoming polarized by the target field. Whereas for the target, the field gradient at the target location is sufficiently low for routine dynamically polarized NH_3 or ND_3 target operation, with a relative values of 0.4×10^{-4}.

The forces between the polarized target and CPS magnets were calculated by using several methods, including an analytical estimate for the 700 kA per coil (four of them in the target) and the observed field gradients. The gradients lead to about a 20-30 Gauss difference in B_x, B_y at the locations of the two sets of coils (transverse to the beam direction). The force F_z (along the beam line) was found to be about 200 N, which is well below the recommended limit of 1000 N. This is the value that should be considered for support structure engineering designs. A similar force analysis for the polarized target magnet configured in a *transverse* (horizontal) orientation of the target field (see Figure 11 (right panel)) shows that the resulting force is slightly lower and the gradient at the target (B_x in this case) is around the same 2 Gauss/cm value.

V Radiation Requirements

As discussed previously, the WACS experiment with the proposed CPS will utilize a dynamically nuclear polarized target. Electron beam currents for use with such targets are typically limited to 100 nA or less, to reduce both heat load and radiation damage effects. The equivalent heat load for a pure photon beam impinging on such a target corresponds to a photon flux originating from a 2.7 μA electron beam current striking a 10% copper radiator. The radiation calculations presented in this section therefore assume a CPS able to absorb 30 kW in total (corresponding to a beam of 11 GeV electrons with a current of 2.7 μA). In addition, the beam time assumed for a typical CPS experiment is 1000 hours (∼40 PAC days).

For such an experiment, the following radiation requirements must be fulfilled:

- The prompt dose rate in the experimental hall must be $\leq$ several rem/hr at a distance of 30 feet from the CPS.

- The prompt dose rate at the site boundary must be $\leq$ 1 μrem/hr. (For comparison, 2.4 μrem/hr is the corresponding rate for a typical Jefferson Lab experiment which does not require extra shielding).

- The activation dose outside the CPS envelope at a distance of one foot must be $\leq$ several mrem/hr one hour after the end of a 1000 hour run.

- The activation dose at the pivot in the experimental target area, where operational maintenance tasks may be required, is dominated by the dose induced by a pure photon beam, and at a distance of one foot from the scattering chamber must be $\leq$ several mrem/hr one hour after the end of a 1000 hour run (i.e. the additional dose induced by radiation of the main beam absorbed in the CPS should be negligible).

The CPS design should combine in a single shielded assembly all elements necessary for the production of the intense photon beam and ensure that the operational radiation dose rates are within the requirements outlined above. Much of this is achieved by keeping the overall dimensions of the CPS as small as possible, by careful choice of materials, and by locating radiation shielding as close to the source of radiation as possible. Compared to a traditional bremsstrahlung photon source, the proposed solution will present several advantages,

including much lower radiation levels, both prompt and post-operational due to the beam line elements radio-activation, as will be shown later in this section.

The CPS conceptual design has been established with extensive and realistic simulations. As validation of the simulation tools used, benchmark comparisons were made with GEANT3, GEANT4, FLUKA and DINREG. The benchmark results are further described in Appendix 2. After benchmark validation, an extensive series of radiation calculations were performed in order to:

- Determine the size and layout of the shielding around the magnet, and the choice of materials (copper, Cu-W alloy, concrete, borated plastic, etc.).
- Determine the magnet field requirements in terms of peak field, gap size, and field length.
- Determine the radiation levels on the magnet coils, and based on these results to identify radiation hardened materials that might be used in building the coils.
- Determine the radiation levels on the polarized target electronics.
- Determine the radiation levels directly adjacent to the CPS as well as at the experimental hall boundary.

The logic behind the CPS hermetic shielding design is that radiation (γ, n) from the source should be a few times less than from a photon beam interacting with the material of a polarized target. The CPS is designed to meet the radiation level requirements specified in Appendix 2 for an electron beam current of 2.7μA (30 kW), run time of 1000 hours, and the photon source as close to the target as possible. The shielding design consists of tungsten powder and 10 cm of 30% borated plastic. The addition of the latter has considerable impact in reducing the neutron flux escaping the CPS, illustrated in Figure 16.

VI Radiation Studies and Shielding Design

In this section we will describe several different configurations for comparison, the first of which is the default situation for dynamically nuclear polarized targets in Hall C and elsewhere, which is that of a 100 nA incident electron beam. The second configuration corresponds to the equivalent photon flux created by a 2.7 μA electron beam on a 10% copper radiator incident on the same polarized target system. In this scenario, we remove all the secondary particles generated in order that it mimics a pure and background-free photon beam. The third scenario is one with the CPS under the same conditions, a 2.7 μA electron beam on a 10% copper radiator, for which all the radiation background is included in the simulation. In some cases we have simulated only the effect of the CPS, while in others the CPS and the target system combined are considered.

A Prompt Radiation Dose without a Target

In order to help introduce the shielding concept of the CPS, we start by comparing the prompt radiation doses as calculated in a ring detector covering a radial range between 5 and 10 cm from the beam line. We first calculate the prompt dose originating from a 2.7 μA electron beam hitting a 10% copper radiator a distance of 2.15 m upstream of the pivot. There is no target system in this simulation, which means that all prompt radiation originates from the interaction between the primary beam and the radiator. Figure 13 shows two-dimensional dose rates originating from photons only (top left), from neutrons only (top right), from all particles (bottom left), and the one-dimensional prompt radiation dose along the beam direction (bottom right). Obviously, except for the neutron contribution most of the prompt radiation is created along the beam direction. The prompt radiation levels reach roughly 40 rem/hr, of which only around 200 mrem/hr is in the form of gamma radiation and 10 mrem/hr from neutrons. The remaining and clearly dominant contribution are the charged electrons and positrons created, inducing further showers.

A striking difference is observed in the case of a 2.7 μA electron beam incident on a 10% copper radiator as before, but now located within the CPS. Figure 14 illustrates the prompt radiation dose along the beam direction. The y-axis scale on this figure is the same as in Figure 13 (bottom right panel). One can therefore clearly see that the prompt radiation (again, in a 5 to 10 cm ring detector along the beam axis) within the CPS is much higher (300 times, because with CPS the full power of the beam is deposited). Crucially, however, the prompt radiation dose outside the CPS is reduced by a factor of over 1000 to roughly 15 mrem/hr.

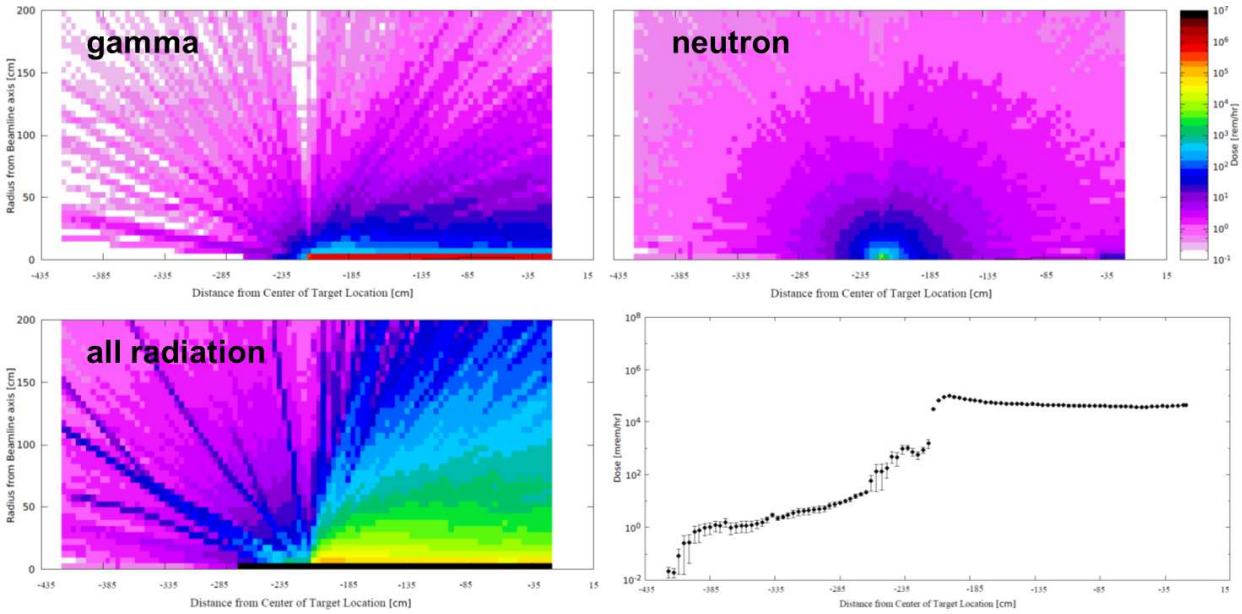

Figure 13: Two-dimensional dose rates as originating from photons only (top left), from neutrons only (top right), from all particles (bottom left) and the (one-dimensional) prompt radiation dose along the beam direction (bottom right).

This factor is entirely consistent with the reduction factor of estimated previously in section IV D.

This extremely important result is further illustrated in Figure 15. In stark contrast with the case without the CPS, there is now no contribution to the prompt dose from photons, electrons and positrons – the neutron-only dose rate is nearly identical to the all-radiation rate. The fourth panel in Figure 15 (bottom right) illustrates how well an optimized CPS shielding concept absorbs the prompt radiation. Outside the CPS the prompt radiation dose rate on the surface (indicated by the outer black rectangular lines) is reduced to a maximum level of roughly 10 rem/hr. This shielding concept is so effective because of the fact that the development of showers generated by interactions of the primary beam is highly suppressed and the resultant secondary particles contained. This confirms that with a CPS the following requirement can be met: **prompt dose rate in hall $\leq$ several rem/hr at 30 feet from device**.

B Impact of Boron and Shielding Optimization

It is well-known that the neutron flux through a surface can be drastically reduced by the addition of boron as a result of the very high capture cross section of ^{10}B. We simulated this effect by calculating the neutron flux at the CPS boundary assuming various thicknesses of tungsten shielding (65, 75 and 85 cm radial), and then adding 10 cm of borated (30%) plastic. The result can be seen in Figure 16, which shows the neutron flux as function of neutron energy (on a logarithmic scale). Adding 10 cm of tungsten clearly reduces the neutron flux as expected, but a much more drastic reduction is seen when the 10 cm of borated plastic is added. Thus, in our design we assume an outer layer of 10 cm-thick borated plastic for the CPS. In order to demonstrate how well the shielding design has been optimized, Figure 17 shows a comparison between the prompt radiation dose rates with the optimized shielding design (right) and with 10 cm less tungsten shielding and no borated plastic (left). (Note that in these panels the CPS magnet is assumed to be at the center of the beam line, in contrast with earlier figures.)

C Prompt Dose Rates at the Boundary

In benchmark calculations assuming spheres of pure shielding materials (see a more extensive description of the benchmark calculations in Appendix 2) we find that the prompt dose rate esti-

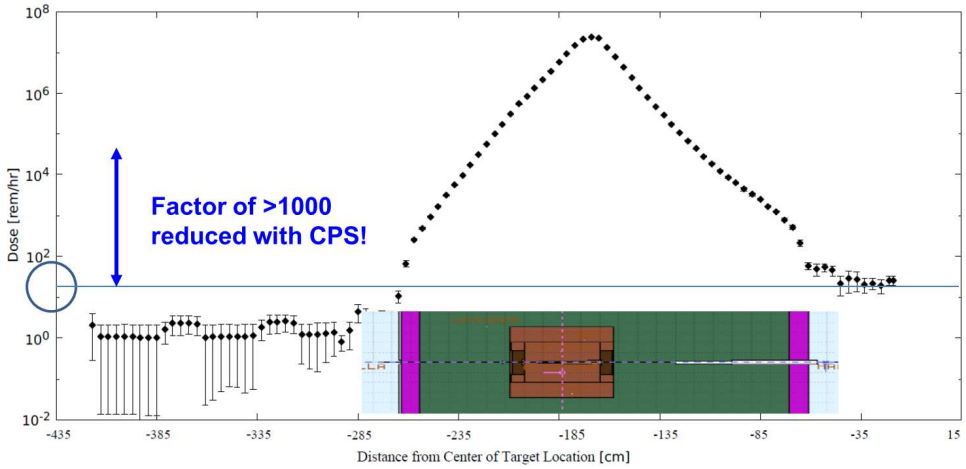

Figure 14: One-dimensional prompt radiation dose along the beam direction, from all particles. The large reduction factor of >1000 induced by the Compact Photon Source design outside the magnet itself is apparent. Along the beam line inside the magnet, the prompt radiation dose can go up to above 10 Mrem/hr, dropping rapidly with distance.

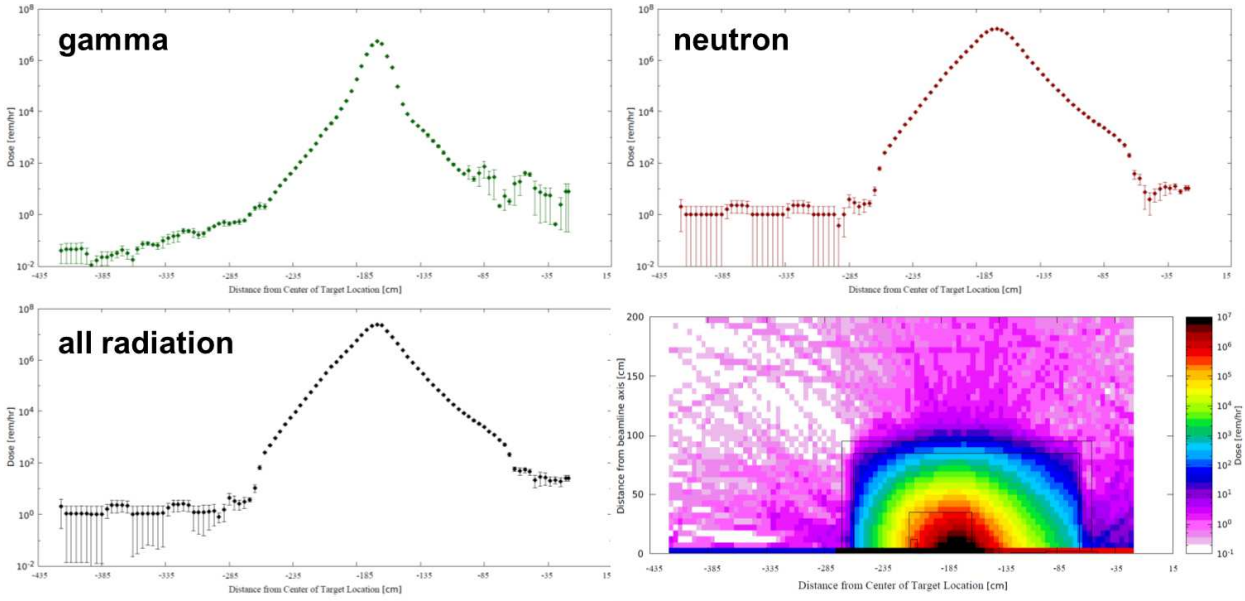

Figure 15: The (one-dimensional) prompt radiation rates as originating from photons only (top left), from neutrons only (top right), and from all radiation sources (bottom left). The fourth panel (bottom right) illustrates how well an optimized CPS shielding concept absorbs the prompt radiation, outside the CPS the prompt radiation is on the surface (indicated by the outer black rectangular lines) already reduced to a level of roughly 10 rem/hour at most.

mates at the RBM-3 boundary are 0.24 μrem/hr for a 3 meter diameter iron sphere and 2.4 μrem/hr for a 1.5 meter diameter tungsten sphere. The baseline design for CPS shielding is assumed to be 85 cm thick tungsten surrounded by 10 cm of borated plastic. Hence, the boundary dose is **below the 2.4 μrem/hr that corresponds to a typical experimental run at Jefferson Lab, for which additional local shielding is not required**. If required, further reductions in the boundary dose can be achieved by optimizing the baseline design in terms of material choice and geometry. Note also that for Hall D, the CPS design is compatible with the site boundary limits as the standard Hall D tagger magnet can dump up to 60 kW in a local beam dump. Indeed, the Hall D

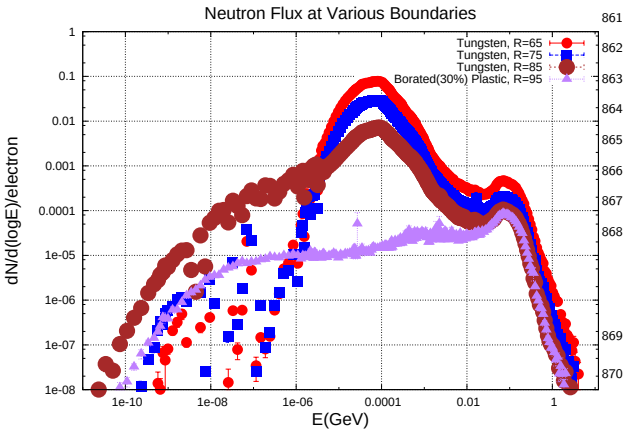

Figure 16: Neutron flux for different shielding configurationsB.

tagger building has been designed assuming a 12 GeV electron beam up to a current of 5 μA. For the CPS, one can thus assume the Hall D tagger magnet building shielding is appropriate in the case for up to 60 kW being dumped in the CPS itself, albeit with the possibility that additional local shielding may be required.

D Activation Dose without a Target

We now turn to the activation dose expected around the CPS following beam-on conditions. Figure 18 shows the calculated activation dose one hour after a 1000-hour experiment has been completed with the same conditions as before (2.7 μA, 10% copper radiator, with shielded CPS). The radiation calculations show the activation dose outside the CPS is reduced to the order of roughly 1 mrem/hr. To quantify this further, Figure 19 shows the activation dose radially away from the CPS. The activation dose outside the CPS is reduced to 2 mrem/hr at the surface and reduces radially outward. At one-foot distance, it is reduced to about 1.5 mrem/hr, while at two-feet distance it is further reduced to less than 1 mrem/hr. Hence, this demonstrates that the current design meets the requirement that **activation dose outside the device envelope at one foot distance is $\leq$ several mrem/h after one hour following the end of a 1000 hour run**.

Note that these estimates do not depend much on the assumed 1000-hour continuous running assumption, as similar dose rates are seen in a calculation for a 100-hour continuous run, reflecting that much of the activation is instant. Furthermore, activation dose rates do not drop appreciably after one hour or even one day. On the other hand, after one month the activation dose rates at the CPS surface will be reduced by up to a factor of ten. Inside the CPS the activation dose rate can be up to 1 krem/hr, which is why the CPS will be moved laterally to the side after an experiment rather than disassembled.

E Radiation Dose Rates with a Target

In building further on our radiation calculations, we have included the polarized target scattering chamber and target system. In Figure 20 we illustrate our setup and show a side-view of the CPS, indicating the magnet, the tungsten-powder shield, the layer of borated plastic, and also the scattering chamber with polarized target system. The description of the scattering chamber and polarized target includes: the exact diameter of the scattering chamber and all the ports with accurate dimensions and window materials; and the polarized target material including the liquid helium surrounding the target beads.

Figure 21 is included here for completeness. It illustrates the 1-MeV neutron equivalent damage to silicon (in neutrons/cm^2), which is the relevant quantity to quantify the risk of radiation damage to sensitive electronics. The result, not surprisingly, shows that there is a narrow cone in the forward direction, along the beam axis, up to roughly one meter, in which sensitive electronics should not be placed if at all possible.

Figure 22 shows the prompt dose at the target for different configurations. The distance R is radial distance from the pivot, with the radius of the scattering chamber boundary at 50 cm. The various colors on the figure represent the various types of configurations studied: the *100 nA electron beam* (red downward triangles), the *2.7 μA photon beam* (blue upward triangles), the *CPS without polarized target* (black circles), and the *CPS with polarized target* (mauve squares). At the boundary of the scattering chamber in the *100 nA electron beam* configuration, the default operating mode for polarized beam experiments with dynamically nuclear polarized targets in Hall C to date, the prompt dose is roughly 1 rem/hr. In the *2.7 μA photon beam* scenario it is roughly 30 rem/hr, which simply reflects the fact that even if a 2.7 μA pure photon beam deposits the same heat load in a target as a 100 nA electron beam, the radiation rate is much higher. The *CPS with polarized target*

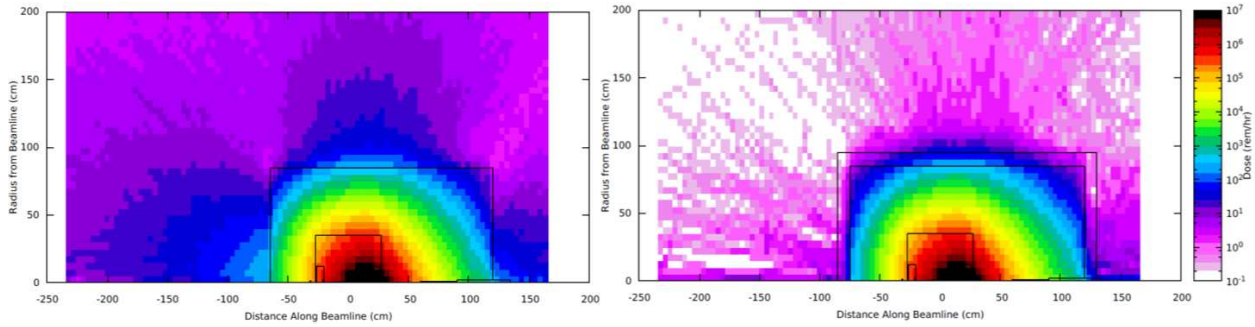

Figure 17: The prompt radiation rates with the optimized shielding design, whereas in the left panel we show the same prompt radiation rates without extra shielding (10 cm less of tungsten shielding, and no borated plastic). Note: these are with the CPS magnet centered around "zero" along the beam line.

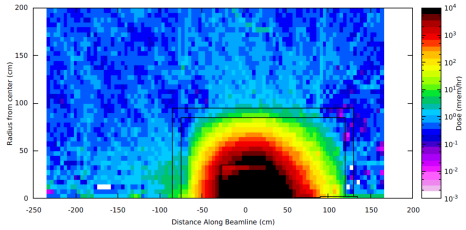

Figure 18: Calculated activation dose one hour after a 1000-hour experiment under the described conditions (2.7 μA, 10% Cu radiator, with shielded CPS) has been completed. Note: these are with the CPS magnet centered around "zero" along the beam line.

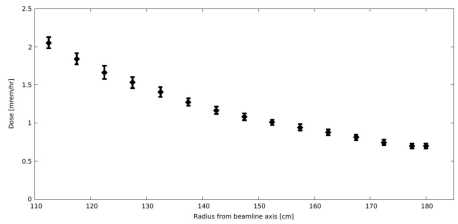

Figure 19: Activation dose outside CPS 1 hour after a 1000 hour run is 2 mr/hr on contact and reduced radially outwards.

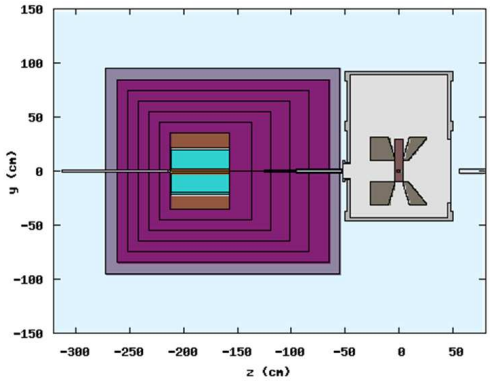

Figure 20: Side view of the Compact Photon Source, indicating the magnet, the W powder shield, and the layer of borated plastic, and also the scattering chamber with polarized target system.

scenario is identical to the pure photon beam case, further demonstrating that no additional radiation comes from the CPS.

Figure 23 is perhaps more instructive, in that it shows the activation dose rates for the same three configurations. The vertical size of the figure panels have been adjusted such that equal dose rates line up from left to right. One directly can see therefore that the *2.7 μA photon beam* configuration has a much higher activation dose rate than the *100 nA electron beam* case. This again reflects what was seen in the previous figure for the prompt radiation dose rate, as there are many more photons coming from a 2.7 μA electron beam on a 10% copper radiator than there are from a 100 nA electron beam on a roughly 3% dynamically nuclear polarized target. More interestingly, the effect of the CPS is again negligible: activation near the target does not come from the CPS itself, but rather from the photon beam we have created. The price to pay is that one ends up with a roughly constant 0.1 mrem/hr activation level at large radial distances, but this is manageable.

We also indicate in the various panels of Figure 23 how quickly the activation rates drop (after one hour, one day, one week, and one month). One can see that much of the 0.1 mem/hr activation level induced by the deployment of the CPS has decayed away after a week. This is consistent with what was observed in the example of the activation levels at radial distances around the CPS above.

Lastly, we illustrate in Figure 24 in a two-dimensional plot the activation dose rates one hour

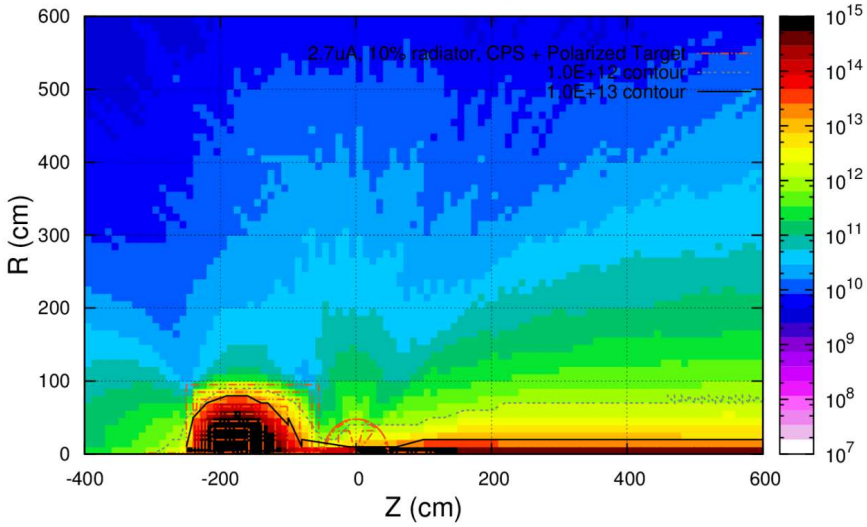

Figure 21: 1-MeV neutron equivalent damage to silicon (in neutrons/cm^2).

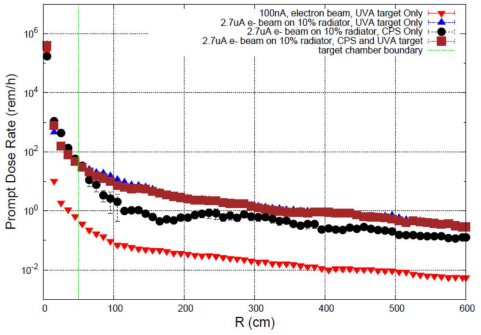

Figure 22: Prompt dose at the target for different configurations. Distance R is radial distance from the pivot, with the radius of the scattering chamber boundary at 50 cm.

after a 1000 hour run with the CPS, a 2.7 μA, 11 GeV beam on a 10% radiator and the polarized target system (at z = 0). The 1 mrem/hour contour is indicated. This demonstrates that with the current CPS baseline design, the **activation dose at the pivot in the experimental target area, where operational maintenance tasks may be required, is dominated by the dose induced by a pure photon beam and is at one-foot distance from the scattering chamber $\leq$ several mrem/hr one hour after a 1000 hour run**, and also that **the additional dose induced by radiation of the main beam absorbed in the CPS is negligible**. These were the last of the radiation requirements that were introduced in section V.

VII Engineering and Safety Aspects

In this section we will describe the engineering and safety aspects of the CPS. We will start with a summary of material considerations taking into account the high radiation and power inside the CPS, folding in further insights of the radiation studies as relevant for materials for the CPS and the dynamically nuclear polarized target. Then we describe various engineering aspects such as cooling and magnetic forces, and some further considerations for assembly and installation of the CPS. We will also shortly outline safety aspects related to the CPS, such as use of interlock systems during CPS operation.

A Material Considerations

The level of radiation of the CPS experiments is well below what is typical for many high-luminosity experiments in Experimental Halls A and C at Jefferson Lab using regular cryogenics target systems and/or radiators. The prompt radiation level on the polarized target is higher than before, which is simply an artefact of the higher photon flux associated with the higher figure-of-merit of the CPS experiments. The radiation level on the polarized target coils, due to the interaction of the photon beam with the polarized target material, amounts to about 500 rem/hr as illustrated in Figure 25. The radiation levels in the CPS mag-

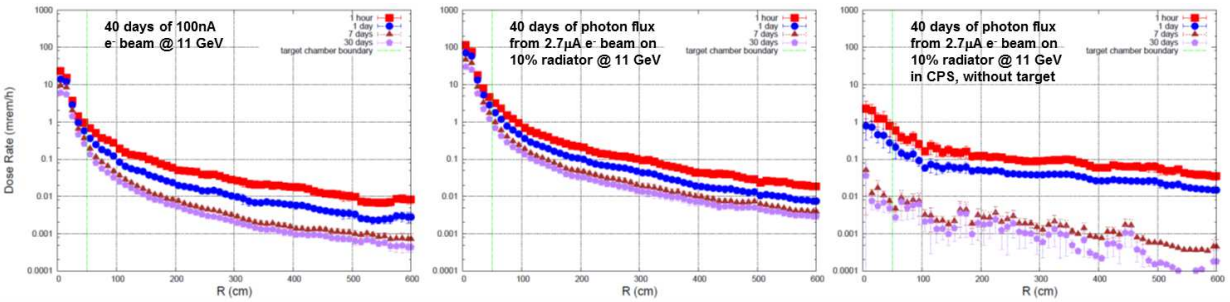

Figure 23: Activation dose rates at the target for different configurations. Distance R is radial distance from the pivot, with the radius of the scattering chamber boundary at 50 cm.

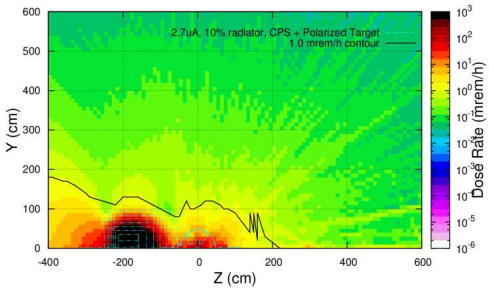

Figure 24: Activation dose rates one hour after a 1000 hour run with the Compact Photon Source, a 2.7 μA beam and a 10% radiator, at 11 GeV beam energy, and the polarized target system (at $z = 0$). The 1 mr/hr contour is indicated. Note that these activation dose rates do not depend much on the assumed 1000-hour continuous run, the rates would be only slightly lower (by 5-10%) and near-identical for a 100-hour continuous run, after one hour.

net coils, at a distance of 20 cm from the radiation source, are reduced to below 1 Mrem/hr (see *e.g.* Figure 15, bottom right), and allow the use of a modest-cost Kapton tape-based insulation of the coils [5].

As described in Section IV B, we explicitly added a small insert of copper within the tungsten-powder shielding of CPS to act as the beam power absorber. The combination of a small $\pm$ 1 mm vertical raster and the magnet field shaping spreads the beam power density over a large surface, such that the temperature of the copper absorber was less than 400°C. This is well below its melting temperature of 1,085°C.

B Cooling and Magnetic Forces

Cooling of the core requires 4 gallons per minute at 110 psi pressure. This will result in a 30°C temperature rise of the cooling water. These values are consistent with provisions in Experimental Hall C at Jefferson Lab, the Hall planned for use for the approved CPS science program. Activation of the cooling water of the CPS magnet and beam dump is likely and a closed-cycle cooling system is planned. Hall C has had secondary in-Hall water-cooled dumps of comparable power before, for polarized target experiments in the 6-GeV era. High-power radiators are also not new and have been used with tens of μA on 10% radiation length targets, also with closed-loop water cooling systems. The magnet heat and dump heat can be removed through a heat exchanger to either the Hall C air or LCW. Any activation of the CPS will be confined to a very small volume and in the event of a leak external contamination will be minimized. A leak pan under the CPS could easily be included to catch and confine any leakage up to and including a total loss of primary coolant. A modular pallet mounted design would be efficient and would include primary coolant pumps, DI resin beds, heat exchanger, surge tank, controls, and instrumentation and manifolds.

The CPS magnet will be located relatively close to the 5 Tesla solenoid of the polarized target whose mutual forces need to be taken into account in the design of the support structure and may require compensation. Preliminary analysis was already performed in a technical note, at that time based on iron-based shielding [2]. In the present design the iron-based shielding is replaced by more effective tungsten-powder shielding, which also much reduces the forces. Residual fields and forces from the CPS magnet will require further iron shielding to avoid interference with the Polarized Target magnet.

Another magnetic consideration is the effect on field quality at the polarized target. The fields and gradients imposed on the polarized target will not be large but they must be compensated at the 10^{-4} level. Some further magneto-static effort to

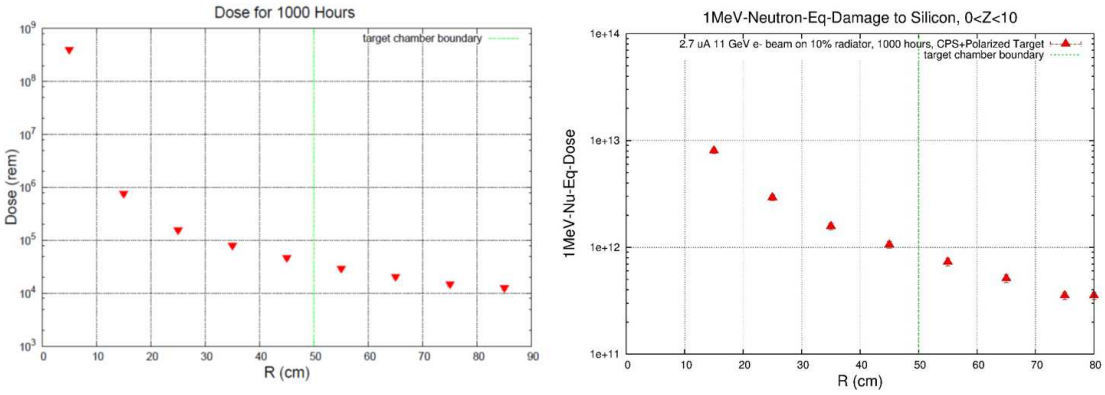

Figure 25: The prompt dose rates (right) and the resulting 1 MeV neutron equivalent damage to silicon (left) in the target area, assuming a 1000 hour run with the Compact Photon Source with a 2.7 mA beam, a 10% Cu radiator, and 11 GeV beam energy. The polarized target system is at z = 0 and the nominal target chamber radius is 50 cm. The target coils are at about 20 cm from the beam line. The dose for 1000 hours of beam time at the target coils is 5 times 10^5 rem and the 1 MeV neutron equivalent damage is 5 times 10^{12} neutrons/cm^2. The contribution of the CPS backgrounds to these numbers is negligible (contributing 2.5% only).

model the target environment and design a compensation system is required.

C Assembly and Installation Considerations

The CPS can be completely pre-assembled before installation. The outer dimension of the CPS tungsten-powder shielding as outlined for optimized shielding (see Figure 17, right panel) is 1.7 m by 1.7 m by 1.95 m, or a volume of 5.63 m^3. From this, one needs to subtract the inner box including the magnet, which amounts to 0.26 m^3. This means a net volume of 5.37 m^3, or 88 tons, for the optimized tungsten-powder shielding presented. In total, the CPS weight is estimated to be 100 tons. Hence, a reinforced floor would be required for CPS assembly.

There are various options to reduce weight and cost, as needed. Note that the cost of the CPS will be dominated by the cost of the shielding materials. One could reduce the overall size of the W-powder shielding by 5 cm on each side. This would imply an increase of the radiation levelswe estimated by about 50%, and a reduction to 4.48 m^3 or 73 tons (for the W-powder). If one would remove an additional 10 cm only on the bottom side, towards the floor, for an additional factor of two increase in radiation level in the direction of the floor, as calculated for the example of Experimenatl Hall C at Jefferson Lab, this reduces to 68 tons. Alternatively, one could round the W-powder box corners, as illustrated in Figure 26. This would complicate modular construction, but would allow to reach similar radiation levels aas with the optimized design, while reducing material needs and weight. To verify this, we updated the FLUKA model originally developed by one of us (Parker Reid (SMU)) to assist the CPS conceptual design, and replaced the W-powder ($\rho = 16.3\, g/cm^3$) with B(5%)-CH_2 in the rounded corners. The result of the FLUKA analysis confirmd that such a configuration can achieve the same level of radiation outside of the CPS as the optimized shielding design model, but with the volume (and weight) of the W-powder reduced by 25%, to ≈66 tons.

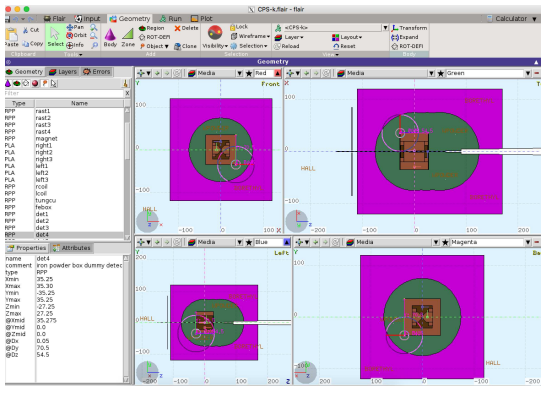

Figure 26: The FLUKA model used in calculations of radiation. Here, front, back, right and left views are shown, illustrating the rounded W-powder (green) corners and the outer borated plastic (purple) volume.

During assembly and after assembly completion the CPS can be measured and fiducialized

to facilitate final alignment. Progressive measurement and fiducialization will eliminate problems with position references becoming hidden. Transporting the CPS to (or within) an Experimental Hall in one piece will preserve the alignment and avoids introduction of errors due to dis-assembly and re-assembly, albeit require temporary use of a large 100-ton truck crane.

When in use for is science experiments, the CPS is expected to become activated and contaminated. Activation levels inside the CPS are expected to be and remain high, until well after experiment completion. Hence, designing the CPS for a one-piece removal limits exposure to staff at the end of the expeirments. The CPS can be left in place, or if removal is required, this task would again require one-time use of a large truck crane to handle the total 100-ton weight of the CPS. The CPS can then be stored. This eliminates the need for staff to dis-assemble the CPS.

Water disconnects using self-sealing connectors can be used to eliminate any primary cooling water loss. The cooling water pumps, controls, DI resin beds and heat exchanger will likely have contaminated water inside but will not otherwise be activated. The cooling pallet can be removed to storage intact or the water drained and stored separately or disposed of. The radiator infrastructure can be similarly stored.

D Equipment Safety and Interlocks

The combination of a high-power radiator, magnet and beam dump inside a shielded box impose reliability and remote handling considerations. The primary engineering controls providing personnel protection are to make the design as robust as possible, with large safety margins, and evade disassembly for maintenance and repair, or equipment removal, altogether.

The CPS should be heavily instrumented for early detection of problems such as low coolant flow, leaks, low pressure, high temperature, and high conductivity. The protection and safety of the CPS begins with the design which must err on the side of conservatism especially in the magnet coil design and dump cooling. A low current density design is envisioned, not to exceed 500 Amps/cm^2. Individual coil pancakes leads should be extended to an area outside of the magnet and shielding for easy access. There should be no electrical or coolant joints inside the CPS shielding. Every separate sub coil of the CPS magnet should have thermometry, klixons and flow measurements to avoid any possibility that one of the separate current paths can overheat due to lack of sufficient coolant, a leak or a bad electrical joint. Voltage monitoring of each sub coil should insure against overheating from any source including internal blockage, leaks, flow restrictions or bad electrical connections. Extra insulation between sub coils and between the coil and ground should be added to prevent ground faults. Lastly, a commercial power supply is assumed and these come with a wide array of internal interlock protections. The available interlocks and signals can be fed into an electron beam Fast Shutdown (FSD) system.

To protect equipment during CPS operations, a dual protection scheme is suggested using both a beam position monitoring system and direct instrumentation of the fast raster magnet itself. The beam diagnostics systems would monitor beam position and motion in close to real time and monitor coild voltage on the raster coils, which would provide ample early warning of raster problems. Both these independent signals would be fed into the FSD system. Radiator temperature could be monitored to provide a third independent protection system, and if implemented, thermocouples mounted on the radiator should be robust against radiation damage and provide fast enough protection against radiator overheating. Simulations of various magnet failure modes such as reduced or no water flow, overheating, etc., can be used to proof test instrumentation and interlocks.

VIII Summary

The Compact Photon Soyrce (CPS) final design features a magnet, a central copper absorber, and hermetic shielding consisting of tungsten powder and borated plastic. The addition of the latter has a considerable impact on reducing the neutron flux escaping the CPS. The ultimate goal in this design process is that radiation from the source should be a few times less than from a photon beam interacting with the material of a polarized target. The equivalent heat load for a pure photon beam impinging such targets corresponds to a photon flux originating from a 2.7 μA electron beam current striking a 10% copper radiator. Detailed simulations of the power density and heat flow analysis show that the maximum temperature in the absorber is below 400 degrees, which is well within the acceptable range of copper, and thus demonstrates that the CPS can absorb 30 kW in total, *e.g.* corresponding to an 11-GeV electron beam energy and a 2.7 μA electron beam current.

The CPS also fulfills the requirements on

operational dose rates at Jefferson Lab (JLab), which have been established with extensive and realistic simulations. The projected prompt dose rate at the site boundary is less than 1 μrem/hr (to be compared with 2.4 μrem/hr, which corresponds to a typical JLab experiment that does not require extra shielding). The activation dose outside the device envelope at one foot distance is less than several mrem/hr after one hour following the end of a 1000 hour run ($\sim$ 3 months). The activation dose at the pivot in the experimental target area, where operational maintenance tasks may be required, is dominated by the dose induced by the pure photon beam. At a distance of one foot from the scattering chamber it is less than several mrem/hr one hour after the end of a 1000 hour run (i.e. the additional activation dose induced by absorption of the electron beam in the Compact Photon Source is negligible).

This document demonstrates that the CPS with an optimized shielding design provides a photon flux of 1.5×10^{12} equivalent photons/s, with a factor of 1000 reduction in prompt radiation dose compared to a 2.7 μA (30 kW) electron beam current striking a 10% copper radiator. The CPS meets the acceptable radiation level requirements for a typical run time of 1000 hours with the photon source located at 2-3m from the target. The technical design and installation in the existing hall infrastructure is feasible.

IX Acknowledgements

We thank Paul Brindza for helpful discussions and providing valuable input for the writing of this document.

---

[1] D. Keller, "The UVa approved and proposed experiments", in arXiv:1704.00816.

[2] B. Wojtsekhowski and G. Niculescu, "Conceptual Design Report, A Compact Photon Source", Supplementary material for the WACS proposal PR12-15-003 to the JLab PAC 43, June 2015; in arXiv:1704.00816.

[3] D. Hamilton, "Photon Beam Requirements for Wide-Angle Compton Scattering", in arXiv:1704.00816.

[4] P.K. Kloeppel, "Design for 25-kW beam dumps at 100 MeV and 500 MeV", CEBAF-TN-90-205; M. Wiseman, C.K. Sinclair, R. Whitney, M. Zarecky, "High Power Electron Beam Dumps at CEBAF".

[5] V.V. Petrov, Yu.A. Pupkov, a report "BINP TESTING OF RADIATION RESISTANCE OF THE MATERIALS USED FOR PRODUCTION OF ACCELERATOR MAGNETIC SYSTEMS", Novosibirsk, 2011

[6] D. Hamilton, D. Day, D. Keller, G. Niculescu, B. Wojtsekhowski, J. Zhang, T. Horn and the Neutral Particle Spectrometer Collaboration, Approved Jefferson Lab experiment E12-17-008. https://misportal.jlab.org/pacProposals/proposals/1353/attachments/08388/Proposal.pdf

[7] M. Boer, D. Keller, V. Tadevosyan, T. Horn and the Neutral Particle Spectrometer Collaboration, Approved Jefferson Lab experiment C12-18-005. https://misportal.jlab.org/pacProposals/proposals/1387/attachments/10437/Proposal.pdf

[8] S. Ali, L. Allison, M. Amaryan, R. Beminiwattha, A. Camsonne, M. Carmignotto, D. Day, P. Degtiarenko, D. Dutta, R. Ent, J.L. Goity, D. Hamilton, O. Hen, T. Horn, C. Hyde, G. Kalicy, D. Keller, C. Keppel, C. Kim, E. Kinney, P. Kroll, A. Larionov, S. Liuti, M. Mai, A. Mkrtchyan, H. Mkrtchyan, C. Munoz-Camacho, J. Napolitano, G. Niculescu, M. Patsyuk, G. Perera, H. Rashad, J. Roche, M. Sargsian, S. Sirca, I. Strakovsky, M. Strikman, V. Tadevosyan, R. Trotta, R. Uniyal, A.H. Vargas, B. Wojtsekhowski, J. Zhang, "Workshop on High-Intensity Photon Sources (HIPS2017) Mini-Proceedings", arXiv:1704.00816 (2017).

[9] [NPS and Experiment Collaboration] S. Abrahamyan, Z. Ahmed, A. Ahmidouch, I. Albayrak, M. Amaryan, D. Androic, K. Aniol, J.R.M. Annand, A. Asaturyan,T. Averett, T. Badman, V. Bellini, M. Ben Ali, F. Benmokthar, J. Bericic, W. Boeglin, M. Boer, W.J. Briscoe, A. Camsonne, M. Canan, M. Capogni, G. Cates, C. Chen, J.P. Chen, M.E. Christy, P. Chu, E. Chudakov, E. Cisbani, S. Covrig, D. Crabb, M. Cummings, . Danagoulian, D. Day, M. Defurne, P. Degtiarenko, A. Del Dotto, J. Denes-Couto, C. Desnault, N. Dien, G. Dodge, M.U. Doering, J. Dunne, R. Dupre, D. Dutta, L. El Fassi, M. Elaasar, R. Ent, C. Fanelli, A. Fradi, G.B. Franklin, S. Frullani, H. Gao, M. Garcon, F. Garibaldi, B. Garillon, D. Gaskell, G. Gavalian, L. Ghedira, R. Gilman, F.X. Girod, D.I. Glazier, J. Gomez, C. Gu, P. Guèye, M. Guidal, J.O. Hamilton, Y. Han, O. Hansen, M. Hattawy, D. Higinbotham, N. Hlavin, T. Horn, M. Huang, G.M. Huber, C.E. Hyde, D.G. Ireland, H.S. Jo, M.K. Jones, N. Kalantarians, D. Keller, J.J. Kelly, C. Keppel, M. Khachatryan, P.M. King, N. Kivel, F. Klein, M. Kohl, P. Kroll, V. Kubarovsky, M. Kunkel, G. Laskaris, W. Li, X. Li, R. Lindgren, J. Liu, K. Livingston, N. Liyanage, E. Long, I.J.D. MacGregor, D. Mack, J. Madsen, F. Mammoliti, V. Mamyan, P. Markowitz, A. Marti Jimenez-Arguello, M. Mazouz, B. McKinnon, M. Metz, M. Meziane, R. Michaels, M. Mi-

hovilovic, G. Miller, A. Mkrtchyan, H. Mkrtchyan, C. Munoz-Camacho, K. Myers, P. Nadel-Turonski, A. Narayan, L. Ndukum, V. Nelyubin, B. Nepal, S. Niccolai, D. Nikolenko, B.E. Norum, F. Noto, Nuruzzaman, M.A. Pannunzio-Carmignotto, M, Paolone, R. Paremuzyan, D. Paudyal, I.L. Pegg, C. Peng, C. Perdrisat, E. Piasetzky, A.J.R. Puckett, V. Punjabi, B. Quinn, I. Rachek, I. Rachet, A. Radyushkin, R. Ransome, M.N.H. Rashad, J, Roche, G. Ron, O. Rondon, F. Sabatie, G. Salme, I. Sapkota, B. Sawatzky, D. Schott, B. Seitz, M.H, Shabestari, A. Shahinyan, Y. Shestakov, S. Sirca, K. Slifer, G. Smith, D. Sokhan, P. Solvignon, S, Stajner, I. Strakovsky, A. Subedi, V. Sulkosky, M.C. Sutera, V. Tadevosyan, L. Tang, J. Tay, lor, M. Ungaro, G.M. Uricuoli, B. Vlahovic, H, Voskanyan, L. Weinstein, F. Wesselmann, B. Wo, jtsekhowski, S.A. Wood, R. Workman, W. Xiong, X. Yan, H. Yao, L. Ye, Z. Ye, M. Yurov, S, Zhamkochyan, J. Zhang, Y. Zhang, R. Zielinski

[10] C. Fanelli, E. Cisbani, D.J. Hamilton, G. Salme, B. Wojtsekhowski, A. Ahmidouch, J.R.M. An, nand, H. Bhagharsayn, J. Baeufait, P. Bosted, E.J. Brash, C. Butuceanu, P. Carter, E. Christy, E. Chudakov, S. Danagoulian, D. Day, P. Degt, yarenko, R. Ent, H. Fenker, M. Fowler, E. Fr, lez, D. Gaskell, R. Gilman, T. Horn, G.M. Hu, ber, C.W. deJager, E. Jensen, Y. Li, R. Lind, gren, H. Lovelace, W. Luo, D. Mack, V. Mamyan, D.J. Margaziotis, P. Markowitz, J. Maxwell, G. Mbianda, D. Meekins, M. Meziane, J. Miller, A. Mkrtchyan, H. Mkrtchyan, J. Mulholland, V. Nelyubin, L. Pentchev, C.F. Perdrisat, E. Pi, asetsky, Y. Prock, A.J.R. Puckett, V. Pun, jabi, M. Shabestari, A. Shahinyan, K. Slifer, G. Smith, P. Solvignon, R. Subedi, F.R. Wessel, mann, S. Wood, Z. Ye, X. Zheng, Phys. Rev. Lett **115** (2015) 152001.

[11] E. Chudakov, D. Day, P. Degtiarenko, R. Ent, D.J. Hamilton, T. Horn, D. Keller, C. Keppel, G. Niculescu, P. Reid, I. Strakovsky, B. Wojt, sekhowski, and J. Zhang, Compact Photon Source Conceptual Design, (2018). Available online: https://wiki.jlab.org/cuawiki/images/4/4f/CPS_document_rev9.pdf

[12] R.L. Anderson et al., Physical Review Letters, **25**, no. 17 (1970), 1218; R.L. Anderson et al., Physical Review D, **14**, no. 3 (1976), 679; G.E. Fischer et al., Nucl. Inst. and Meth. **78** (1970), 25; Y.S. Tsai and V. Whitis, Physical Review, **149**, no. 4 (1966), 1248.

[13] N.R.S. Tait, Nuclear Instruments and Methods **67** (1969) 56; T.A. Armstrong et al., Physical Review D, Volume **5**, Number 7, (1972); A. Jackson, Nuclear Instruments and Methods **129** (1975) 73.

[14] G.R. Court et al., Nuclear Instruments and Methods **177** (1980) 281.

[15] G.G. Crabb, W. Meyer, Ann. Rev. Nucl. Part. Sci **47** (1997) 67.

[16] B. Wojtsekhowski, D. Day, et al., PR05-101 (2005); P. Achenbach et al., MAMI-C.

[17] D. Boer, M. Diehl, R. Milner, R. Venugopalan, W. Vogelsang, A. Accardi, E.C. Aschenauer, M. Burkhardt, R. Ent, V. Guzey, D. Hasch, K. Kumar, M.A.C. Lamont, Y. Li, W. Marciano, C. Marquet, F. Sabatie, M. Stratmann, F. Yuan, S. Abeyratne, S. Ahmed, C. Aidala, S. Alekhin, M. Anselmino, H. Avakian, A. Bachetta, J. Bartels, H. BC, J. Beebe-Wang, S. Belomestnykh, I. Ben-Zvi, G. Beuf, J. Blumlein, M. Blaskiewicz, A. Bogacz, S.J. Brodsky, T. Burton, R. Calaga, Z. Chang, I.O. Cherednikov, P. Chevtsov, G.A. Chirilli, C. Ciofi degli Atti, I.C. Cloet, A. Cooper-Sarkar, R. Debbe, Ya. Derbenev, A. Deshpande, F. Dominguez, A. Dumitru, R. Dupre, B. Erdelyi, C. Faroughy, S. Fazio, A. Fedotov, J.R. Forshaw, R. Geraud, K. Gallmeister, L. Gamberg, J.-H. Gao, D. Gassner, F. Gelis, G.P. Gilfoyle, G. Goldstein, K. Golec-Biernat, V.P. Goncalves, M. Gonderinger, M. Guzzi, P. Hagler, H. Hahn, L. Hammons, Y. Hao, P. He, T. Horn, W.A. Horowitz, M. Huang, A. Hutton, B. Jager, W. Jackson, A. Jain, E.C. Johnson, Z.-B. Kang, L.P. Kaptari, D. Kayran, J. Kewisch, Y. Koike, A. Kondratenko, B.Z. Kopeliovich, Y.V. Kovchegov, G. Krafft, P. Kroll, S. Kumano, K. Kumericki, T. Lappi, T. Lautenschlager, R. Li, Z.-T. Liang, V.N. Litvinenko, S. Liuti, Y. Luo, D. Mueller, G. Mahler, A. Majumder, S. Manikonda, F. Marhauser, G. McIntyre, M. Meskauskas, W. Meng, A. Metz, C.B. Mezzetti, G.A. Miller, M. Minty, S.-O. Moch, V. Morozov, U. Mosel, L. Motyka, H. Moutarde, P.J. Mulders, B. Musch, P. Nadel-Turonski, P. Nadolsky, F. Olness, P.N. Ostrumov, B. Parker, B. Pasquini, K. Passek-Kumericki, A. Pikin, F. Pilat, B. Pire, H. Pirner, C. Pisano, E. Pozdeyev, A. Prokudin, V. Ptitsyn, X. Qian, J.-W. Qiu, M. Radici, A. Radyushkin, T. Rao, R. Rimmer, F. Ringer, S. Riordan, T. Rogers, J. Rojo, T. Roser, R. Sandkapen, R. Sassot, T. Satogata, H. Sayed, A. Schafer, G. Schnell, P. Schweitzer, B. Sheehy, J. Skaritka, G. Soyez, M. Spata, H. Spiesberger, A.M. Stasto, N.G. Stefanis, M. Strikman, M. Sullivan, L. Szymanowski, K. Tanaka, S. Taneja, S. Tepikian, B. Terzic, Y. Than, T. Toll, D. Trbojevic, E. Tsentalovich, N. Tsoupas, K. Tuchin, J. Tuozzolo, T. Ullrich, A. Vossen, S. Wallon, G. Wang, H. Wang, X.-N. Wang, S. Webb, C. Weiss, Q,. Wu, B.-W. Xiao, W. Xu, B. Yunn, A. Zelenski, Y. Zhang, J. Zhou, and P. Zurita, "Gluons and the quark sea at high energies: Distributions, polarization, tomography", INT-PUB-11-034,BNL-96164-2011,JLAB-THY-11-1373, August 2011.

[18] A.J.R. Puckett, E.J. Brash, M.K. Jones, W. Luo, M. Meziane, L. Pentchev, C.F. Perdrisat, V. Punjabi, F.R. Wesselmann, A. Ahmidouch, I. Albayrak, K.A. Aniol, J. Arrington, A. Asaturyan, H. Baghdasaryan, F. Benmokthar, W. Bertozzi, L. Bimbot, P. Bosted, W. Boeglin, C. Butuceanu, P. Carter, S. Chernenko, E. Christy, M. Com-

misso, J.C. Cornejo, S. Covrig, S. Danagoulian, A. Daniel, A. Davidenko, D. Day, S. Dhamija, D. Dutta, R. Ent, S. Frullani, H. Fenker, E. Frlez, F. Garibaldi, D. Gaskell, S. Gilad, R. Gilman, Y. Goncharenko, K. Hafidi, D. Hamilton, D.W. Higinbotham, W. Hinton, T. Horn, B. Hu, J. Huang, G.M. Huber, E. Jensen, C. Keppel, M. Khandaker, P. King, D. Kirillov, M. Kohl, V. Kravtsov, G. Kumbartzki, Y. Li, V. Mamyan, D.J. Margaziotis, A. Marsh, Y. Matulenko, J. Maxwell, G. Mbianda, D. Meekins, Y. Melnik, J. Miller, A. Mkrtchyan, H. Mkrtchyan, B. Moffit, O. Moreno, J. Mulholland, A. Narayan, S. Nedev, Nuruzzaman, E. Piasetzky, W. Pierce, N.M. Piskunov, Y. Prok, R.D. Ransome, D.S. Razin, P. Reimer, J. Reinhold, O. Rondon, M. Shabestari, A. Shahinyan, K. Shestermanov, S. Sirca, I. Sitnik, L. Smykov, G. Smith, L.Solovyev, P. Solvignon, R. Subedi, E. Tomasi-Gustafsson, A. Vasiliev, M. Veilleux, B.B. Wojtsekhowski, S. Wood, Z. Ye, Y. Zanevsky, X. Zhang, Y. Zhang, X. Zheng, and L. Zhu, "Recoil Polarization Measurements of the Proton Electromagnetic Form Factor Ratio to $Q^2 = 8.5$ GeV^2", Phys. Rev. Lett. **104**, 242301 (2010).